Available online at www.sciencedirect.com
SCIENCE DIRECT®
ELSEVIER
Journal of Computational and Applied Mathematics 192 (2006) 282–300
JOURNAL OF COMPUTATIONAL AND APPLIED MATHEMATICS
www.elsevier.com/locate/cam

Chemotactic and diffusive migration on a nonuniformly growing domain: numerical algorithm development and applications

Matthew J. Simpson[a,*], Kerry A. Landman[a], Donald F. Newgreen[b]

[a]*Department of Mathematics and Statistics, University of Melbourne, Vic. 3010, Australia*
[b]*The Embryology Laboratory, The Murdoch Childrens Research Institute, Royal Children's Hospital, Parkville, Vic. 3052, Australia*

Received 22 September 2004; received in revised form 2 May 2005

Abstract

A numerical algorithm to simulate chemotactic and/or diffusive migration on a one-dimensional growing domain is developed. The domain growth can be spatially nonuniform and the growth-derived advection term must be discretised. The hyperbolic terms in the conservation equations associated with chemotactic migration and domain growth are accurately discretised using an explicit central scheme. Generality of the algorithm is maintained using an operator split technique to simulate diffusive migration implicitly. The resulting algorithm is applicable for any combination of diffusive and/or chemotactic migration on a growing domain with a general growth-induced velocity field. The accuracy of the algorithm is demonstrated by testing the results against some simple analytical solutions and in an inter-code comparison. The new algorithm demonstrates that the form of nonuniform growth plays a critical role in determining whether a population of migratory cells is able to overcome the domain growth and fully colonise the domain.

Keywords: Chemotaxis; Diffusion; Cell migration; Growing domain; Nonuniform growth; Central scheme; Operator splitting; Hirschsprung's disease

* Corresponding author. Tel.: +613 8344 6517; fax: +613 8344 4599.
E-mail address: m.simpson@ms.unimelb.edu.au (M.J. Simpson).

0377-0427/$ - see front matter © 2005 Elsevier B.V. All rights reserved.
doi:10.1016/j.cam.2005.05.003

1. Introduction

Cell migration occurs over many scales and is initiated for a wide variety of reasons [30]. For example, single cell organisms can respond to external stresses by moving through their environment for survival. Multi-cellular organisms rely on cell migration as a mechanism for development, repair and immune responses. Several mechanisms for cell migration have been postulated. Diffusion, whereby cells undergo a random walk, is the classical conceptual model for cell migration [12,23]. Cells can also move in response to a gradient of an external signal. For example, the external signal may be a signalling chemical (typically a diffusible molecule), an adhesive extra-cellular matrix molecule or a magnetic field. These mechanisms are called chemotaxis, haptotaxis and magnetotaxis, respectively. A population of bacteria can move through its environment via chemotaxis [1,16] or magnetotaxis [5], optimising nutrient uptake. Chemotaxis of single cells and cell populations is well studied [34,45]. Angiogenisis [2] and tumor cell invasion are mediated by haptotaxis and chemotaxis [3,33,44].

Biological development processes are often associated with physical expansion and growth as in embryogenesis of reptiles, birds, mammals and fish where development occurs in the presence of an extra-embryonic nutrient source. Under certain circumstances, biological growth and migration occur simultaneously and at comparable rates such that each can influence the other. General problems combining biological growth and migration encompass a broad range of processes including both cellular migration and the migration of biochemical signalling species. For example, the development of biological patterns are thought to arise through the migration of an activator–inhibitor biochemical signalling system within expanding tissues [6,7]. Localised apical growth [10,26,32] and nonlocalised domain expansion [8,18,21,28,38] have been considered as specific types of domain growth relevant to particular biological systems.

Mathematical models of biological pattern development have been predominantly concerned with diffusive migration on uniformly expanding domains undergoing slow growth [7,35]. Typically the numerical approach to solving these systems uses a moving grid [38] or a transformed grid [7] upon which the governing equations are discretised.

Simulating migration on a transformed domain undergoing spatially uniform expansion is a particular case of a more general problem. For uniform growth, the hyperbolic terms associated with domain growth and the transformation to the fixed coordinate system are equal and opposite. Therefore, these terms cancel and are not discretised. For the more general problem of migration on a non-uniformly growing domain all terms must be accurately discretised.

In addition to biological applications, there is a broader research interest in migration processes on growing domains. In polymer science the dynamics of material swelling associated with solute migration has several theoretical and industrial applications [13]. Similarly in health sciences, solute migration within swelling tissues is of interest to understand biochemical responses to injury [40]. Therefore, an ability to mathematically model migration on growing domains is of broad interest.

This work presents a numerical algorithm for simulating diffusive and/or chemotactic migration on a growing domain where the domain growth can be spatially non-uniform. Although the particular application that motivated the development of this algorithm involves cell migration by chemotaxis, the algorithm is also applicable to haptotactic migration as chemotaxis and haptotaxis are mathematically equivalent [27]. The algorithm was devised to extend the analysis of the cell migration and colonisation problem posed in [21], which investigated the conditions under which a population of chemotactically motile cells could colonise a growing domain. This previous study was limited to uniform growth. Furthermore, the

numerical scheme used to solve the chemotaxis-dominated problem required an ad hoc addition of linear diffusion to avoid numerical errors [21]. These limitations are completely overcome with the numerical scheme presented here. For this work, the conservation equations are solved with an operator split (OS) strategy [22,42,43], where the central scheme proposed by Kurganov and Tadmor (KT) [19] is used to simulate the hyperbolic and kinetic terms, while the diffusive migration is solved with an implicit finite element (FE) algorithm. The numerical algorithm is applied to a new biologically motivated nonuniform domain growth model. The growth model concerns the rostral-to-caudal migration of neural crest cells in the developing gut during vertebrate embryogenesis. The results illustrate the complex interactions between chemotactic migration and nonuniform growth dynamics.

2. Algorithm development

A system of conservation equations for chemotactic and diffusive migration on a growing domain will be proposed. In developing the numerical algorithm, we emphasise the particular difficulties associated with the terms in the conservation equations and also highlight how the algorithm extends previous attempts at solving related problems. The accuracy and generality of the algorithm is demonstrated via a suite of test cases including a new application relevant to the formation of the vertebrate enteric nervous system.

2.1. Conservation equations for migration on a growing domain

To simulate chemotactic and diffusive migration on a growing domain, conservation of mass equations for the migratory population n and the chemoattractant g can be derived [21]:

$$\frac{\partial n}{\partial t} = \frac{\partial}{\partial x}\left(D_n \frac{\partial n}{\partial x}\right) - \frac{\partial}{\partial x}\left(\chi n \frac{\partial g}{\partial x}\right) - \frac{\partial}{\partial x}(vn) + k_n(n, g), \tag{1}$$

$$\frac{\partial g}{\partial t} = \frac{\partial}{\partial x}\left(D_g \frac{\partial g}{\partial x}\right) - \frac{\partial}{\partial x}(vg) + k_g(n, g), \tag{2}$$

where k_n and k_g are general kinetic functions representing processes that might include mitotic production, differentiation, chemoattractant production and decay, and cell–chemoattractant binding. The velocity v represents the domain growth and will be specified later. The numerical algorithm is not sensitive to the particular form of the kinetic functions. The remainder of this study focusses upon two specific forms of interest [22]:

$$k_n(n, g) = \lambda_1 n\left(1 - \frac{n}{N}\right), \tag{3}$$

$$k_g(n, g) = \lambda_2 - \lambda_3 g - \lambda_4 n g. \tag{4}$$

The choice of kinetic functions represents logistic growth for the proliferation of n, zeroth order production of g, first order decay of g and a nonlinear cell–chemoattractant binding term. These particular kinetics are relevant for the migration of neural crest cells along the growing gut during vertebrate embryogenisis [22]. Neural crest cells respond chemotactically to growth factors, such as Glial-derived neurotrophic factor (GDNF), which is produced within the developing gut [29,46]. Spatial gradients of GDNF are

thought to arise primarily through GDNF binding to receptors on the neural crest cells thereby enabling a localised population of neural crest cells to generate a chemotactic gradient and migration velocity. GDNF also acts as a survival factor for the neural crest cells; consequently cells can only survive where GDNF is present [15,29,46]. Our interest in this system is to predict whether a population of motile cells can colonise a non-uniformly growing domain, such as the developing gut. This problem has relevance to a common birth defect in humans called Hirschsprung's disease, where the migrating neural crest cells fail to completely colonise the growing gut [21,46].

Introducing the dimensionless variables:

$$n^* = \frac{n}{N}, \quad x^* = \frac{x}{L_0}, \quad v^* = \frac{v}{L_0\lambda_1}, \quad g^* = \frac{\lambda_3 g}{\lambda_2}, \quad t^* = \lambda_1 t, \tag{5}$$

where L_0 is the initial length of the domain, we can identify the dimensionless constants:

$$D_n^* = \frac{D_n}{\lambda_1 L_0^2}, \quad D_g^* = \frac{D_g}{\lambda_1 L_0^2}, \quad \chi^* = \frac{\chi\lambda_2}{\lambda_1\lambda_3 L_0^2}, \quad \beta = \frac{\lambda_3}{\lambda_1}, \quad \gamma = \frac{N\lambda_4}{\lambda_1}. \tag{6}$$

Using (5)–(6) without the asterisk notation, the governing equations become

$$\frac{\partial n}{\partial t} = \frac{\partial}{\partial x}\left(D_n \frac{\partial n}{\partial x}\right) - \frac{\partial}{\partial x}\left(\chi n \frac{\partial g}{\partial x}\right) - \frac{\partial}{\partial x}(vn) + n(1-n), \tag{7}$$

$$\frac{\partial g}{\partial t} = \frac{\partial}{\partial x}\left(D_g \frac{\partial g}{\partial x}\right) - \frac{\partial}{\partial x}(vg) + \beta(1-g) - \gamma n g. \tag{8}$$

The objective of this study is to develop an efficient and accurate numerical algorithm to solve (7)–(8). The algorithm must be applicable to either diffusive migration (χ=0), chemotactic migration (D_n=0), diffusive or nondiffusive chemoattractant conditions ($D_g \geqslant 0$), or any combination of diffusion and chemotaxis. In addition, any form of the domain growth velocity v should be permitted.

2.2. Domain growth: relating growth velocity and domain expansion

The domain of interest is $0 < x < L(t)$, where $L(t)$ is the increasing length of the domain. A velocity field causes a point at location x to move to $x + v(x,t)\Delta t$, over the small time period Δt. Considering the expansion of an element Δx, the expression linking the expansion of the total length L to the velocity is

$$\frac{\mathrm{d}L}{\mathrm{d}t} = \dot{L} = \int_0^{L(t)} \frac{\partial v}{\partial x}\,\mathrm{d}x. \tag{9}$$

The key step in defining the growth is specifying the local expansion rate $\partial v/\partial x$. Most previous analyses invoke spatially uniform growth, which means that $\partial v/\partial x$ is independent of position (but not necessarily independent of time) [6,7,21,35]. Here we show that this uniform growth assumption turns out to be the simplest case of a more general problem. We will demonstrate the interesting and important influence of nonuniform growth on migration by considering two examples of this type.

2.3. Transformation to a fixed grid

The conservation equations for n and g are valid on $0 < x < L(t)$. The spatial variable is transformed as $\xi = x/L$ [7,21,35], thereby fixing the domain as $0 < \xi < 1$. This leads to the transformed conservation system:

$$\frac{\partial n}{\partial t} = \frac{\partial}{\partial \xi}\left(\frac{D_n}{L^2}\frac{\partial n}{\partial \xi}\right) - \frac{\partial}{\partial \xi}\left(\frac{\chi}{L^2} n \frac{\partial g}{\partial \xi}\right) - \frac{\partial}{\partial \xi}\left(\frac{1}{L} vn\right) + n(1-n) + \frac{\xi \dot{L}}{L}\frac{\partial n}{\partial \xi}, \tag{10}$$

$$\frac{\partial g}{\partial t} = \frac{\partial}{\partial \xi}\left(\frac{D_g}{L^2}\frac{\partial g}{\partial \xi}\right) - \frac{\partial}{\partial \xi}\left(\frac{1}{L} vg\right) + \beta(1-g) - \gamma n g + \frac{\xi \dot{L}}{L}\frac{\partial g}{\partial \xi}. \tag{11}$$

System (10)–(11) is closed by specifying initial and boundary conditions for n and g and the velocity distribution $v(\xi, t)$. Note that the transformed system (10)–(11) contains additional hyperbolic terms. The significance of these terms will be discussed, especially when comparing the numerical algorithm developed here with previous attempts at solving similar problems.

2.4. Operator split scheme

The OS scheme is now introduced. In each time step the temporal integration is done in two stages [22,42,43]. Firstly, the hyperbolic and kinetic terms are solved using the KT central scheme:

$$\frac{\partial n}{\partial t} = -\frac{\partial}{\partial \xi}\left(\frac{\chi}{L^2} n \frac{\partial g}{\partial \xi}\right) - \frac{\partial}{\partial \xi}\left(\frac{1}{L} vn\right) + n(1-n) + \frac{\xi \dot{L}}{L}\frac{\partial n}{\partial \xi}, \tag{12}$$

$$\frac{\partial g}{\partial t} = -\frac{\partial}{\partial \xi}\left(\frac{1}{L} vg\right) + \beta(1-g) - \gamma n g + \frac{\xi \dot{L}}{L}\frac{\partial g}{\partial \xi}. \tag{13}$$

For the second stage, the remaining diffusion terms are solved using a standard linear mass-lumped FE (or equivalently, a standard linear finite difference) approximation:

$$\frac{\partial n}{\partial t} = \frac{\partial}{\partial \xi}\left(\frac{D_n}{L^2}\frac{\partial n}{\partial \xi}\right), \tag{14}$$

$$\frac{\partial g}{\partial t} = \frac{\partial}{\partial \xi}\left(\frac{D_g}{L^2}\frac{\partial g}{\partial \xi}\right). \tag{15}$$

Within each time step the diffusion terms (14)–(15) are solved using the results from the solution of the first stage (12)–(13) as the initial conditions. With these two steps completed, the whole system (10)–(11) has been advanced through the time step, and the entire procedure is repeated until the desired output time is reached. Further details of this splitting scheme are addressed in [42].

2.4.1. Kurganov–Tadmor central scheme

The KT central scheme has enjoyed recent popularity solving hyperbolic problems such as open channel flow [14], particle settling [4], cell migration [22] and reactive chemical transport in aquifer systems [42]. Because the algorithm is explained in detail elsewhere [14,19,42], only the framework specific to the implementation of KT for the current problem is outlined.

To apply the KT scheme, the conservation system must be in the form

$$\frac{\partial \mathbf{W}}{\partial t} + \frac{\partial \mathbf{F}(\mathbf{W})}{\partial \xi} = \mathbf{Z}(\mathbf{W}), \tag{16}$$

where $\mathbf{W}$ is the vector of conserved variables, $\mathbf{F}$ is the flux and $\mathbf{Z}$ is the vector of kinetic terms. Introducing $h(\xi, t) = \partial g/\partial \xi$ and rearranging the domain growth terms in (12)–(13), the components of (16) are identified:

$$\mathbf{W} = \begin{bmatrix} n \\ g \\ h \\ v \\ \xi \\ \dfrac{\partial v}{\partial \xi} \end{bmatrix}, \quad \mathbf{F} = \begin{bmatrix} \dfrac{\chi n h}{L^2} + \dfrac{nv}{L} - \dfrac{n\xi \dot{L}}{L} \\ 0 \\ -\beta(1-g) + \gamma n g + \dfrac{g}{L}\dfrac{\partial v}{\partial \xi} + \dfrac{vh}{L} - \dfrac{\xi \dot{L} h}{L} \\ 0 \\ 0 \\ 0 \end{bmatrix},$$

$$\mathbf{Z} = \begin{bmatrix} n(1-n) - \dfrac{n\dot{L}}{L} \\ \beta(1-g) - \gamma n g - \dfrac{g}{L}\dfrac{\partial v}{\partial \xi} - \dfrac{vh}{L} + \dfrac{\xi \dot{L} h}{L} \\ 0 \\ 0 \\ 0 \\ 0 \end{bmatrix}. \tag{17}$$

Note that v, ξ and $\partial v/\partial \xi$ are included in formulation (16) even though these terms are not associated with a conservation equation. Maintaining these terms in conservation form enables the KT algorithm to properly account for spatial gradients of these quantities. This is similar to recent work in [4], which provides further discussion on this topic.

The KT algorithm is applied to (16) by computing derivatives using a MINMOD limiter, with $\theta = 1.99$ [42], on a uniformly discretised domain. To perform the temporal integration, the KT algorithm permits a semi-discrete form

$$\frac{\mathrm{d}\mathbf{W}}{\mathrm{d}t} = \mathbf{\Lambda}(\mathbf{W}) + \mathbf{Z}(\mathbf{W}), \tag{18}$$

where $\mathbf{\Lambda}$ represents the spatial discretisation procedure. An explicit 3rd order TVD Runge–Kutta method [39] is used to integrate (18). The stability of this method is subject to the Courant condition, $Cr = \max_i \mid \lambda_i \mid \Delta t/\Delta \xi < 1$, where λ_i are the eigenvalues of the Jacobian of $\mathbf{F}$ [39]. Therefore, Δt must be sufficiently small to satisfy this constraint.

2.4.2. *Galerkin finite element solution of the diffusion equation*

Once the hyperbolic system (12)–(13) is solved, these results are used as initial conditions to solve the remaining diffusion system (14)–(15). The diffusion equations are solved with a mass-lumped linear

Galerkin FE method applied to the same spatial grid. We note that the mass-lumped linear Galerkin FE approximation at a central node is identical to a standard linear finite difference approximation. Temporal integration is performed with the unconditionally stable backward Euler method [9]. The details of the numerical procedure are standard and described elsewhere [37]. In cases where $D_g > 0$, the new solution for $g(\xi, t)$ is then used to update the $h(\xi, t) = \partial g/\partial \xi$ profile. For cases where $D_g = 0$, this update is unnecessary.

The algorithm description is now complete and will be referred to as the Kurganov–Tadmor operator split (KT-OS) algorithm. Before using the algorithm it is prudent to test the accuracy of the scheme. First, the fundamental KT-OS algorithm is tested on a problem with an analytical solution. Second, the KT-OS algorithm is used to solve a combined diffusion and chemotaxis problem on a non-uniformly growing domain and the results are checked with a standard FE algorithm. The inter-code comparison is restricted as the FE algorithm is constrained by the Peclet number [47]. In Section 3, an uncoupled test case is conducted under nonuniform growth conditions that permits part of the conservation system to be solved analytically. This suite of test problems provides confidence in the accuracy of the KT-OS scheme. In addition, the benchmarking procedure allows us to glean some insight into the complex interactions involved in simulating chemotactic and diffusive migration on a nonuniformly growing domain.

2.5. Operator splitting: testing with a Gaussian hill problem

To demonstrate the accuracy of the KT-OS algorithm, a linear advection diffusion equation (ADE) on a nongrowing domain is considered:

$$\frac{\partial c}{\partial t} = D\frac{\partial^2 c}{\partial x^2} - u\,\frac{\partial c}{\partial x}. \tag{19}$$

The application of the KT-OS to (19) is straightforward. Firstly, given initial conditions, the hyperbolic part is advanced over Δt using the KT algorithm. The propagation speed is the imposed velocity, $\lambda = u$. Secondly, the diffusive term is advanced over Δt using the FE algorithm with the results from the KT algorithm as the initial conditions. Further analysis of the OS scheme is given in [42].

Although the ADE is simpler than the cell migration model, the accuracy of the numerical solution depends upon the accuracy of the KT algorithm combined with the OS step. The ADE is ideal for testing the numerical scheme as analytical solutions exist. Here we solve (19) on $-\infty < x < \infty$ with

$$c(x, 0) = \exp\left\{-\left(\frac{x - x_0}{l}\right)^2\right\}. \tag{20}$$

Eq. (19) with the initial condition (20) is known as a Gaussian hill problem [11,42]. The analytical solution is

$$c(x, t) = \frac{1}{\sigma(t)}\exp\left\{-\left(\frac{x - x_0 - ut}{l\sigma(t)}\right)^2\right\},$$

$$\sigma(t) = \sqrt{1 + \frac{4Dt}{l^2}}. \tag{21}$$

Numerical solutions are generated on a truncated domain $0 < x < 2$, with $c(0, t) = c(2, t) = 0$. To illustrate the flexibility of the splitting approach, we use a wide range of diffusion coefficients. With the Peclet

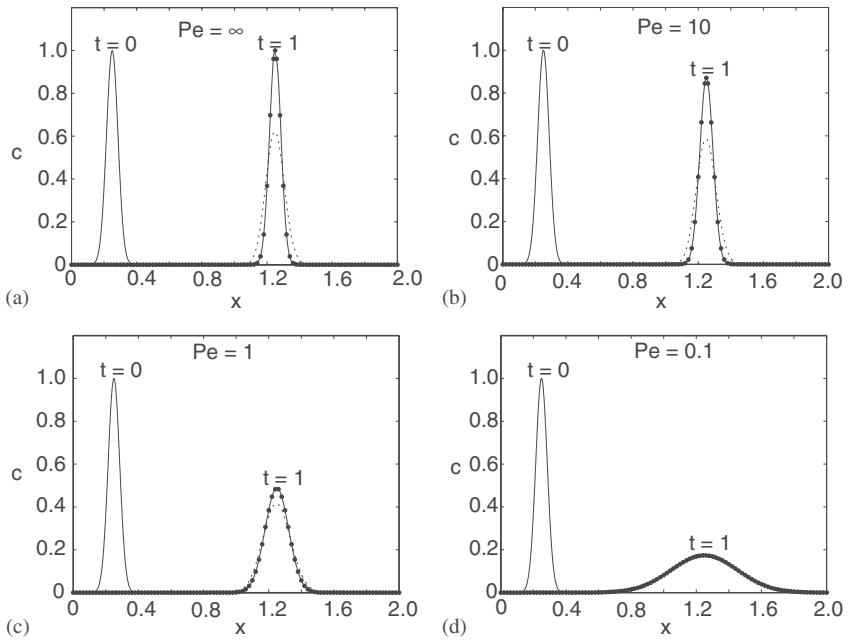

Fig. 1. Comparison of KT-OS (solid line), FE (dotted line) and analytical (•) solutions for the Gaussian hill problem at $t = 1$. A range of Peclet number conditions are shown, (a) $Pe = \infty$, (b) $Pe = 10$, (c) $Pe = 1$ and (d) $Pe = 0.1$. Here $u = 1$, $x_0 = \frac{1}{4}$ and $l = \frac{1}{20}$. Numerical computations are performed with $\Delta x = \Delta t = 2 \times 10^{-3}$.

number defined as $Pe = u\Delta x/D$, we investigate the range of conditions $0.1 \leqslant Pe \leqslant \infty$. Numerical and analytical solutions are compared in Fig. 1.

The numerical results for the Gaussian hill problem indicate that the KT-OS algorithm is able to replicate the analytical solution over a wide range of conditions. The algorithm performs well where there is pure advection and $Pe = \infty$ (Fig. 1a). This is expected as no splitting is required. More importantly, the numerical profiles are also accurate when splitting is invoked (Fig. 1b–d). In addition, an implicit mass-lumped FE (centered finite difference) algorithm was also used and the results are shown in Fig. 1. For high Peclet numbers the FE solution performs poorly; the profiles are excessively dissipative and the peak concentration is severely underestimated. As well as the results shown here, further tests were conducted incorporating linear decay into the ADE. These additional simulations were performed under identical conditions as for the conservative Gaussian hill problem. The numerical results accurately reproduced the analytical profiles, thereby illustrating the generality of the proposed solution scheme [42].

Splitting the diffusion term and solving it implicitly are necessary to simulate the wide range of results given in Fig. 1 using a fixed discretisation and a single algorithm. For example, if the diffusion terms were discretised explicitly in the KT algorithm then the OS step could be avoided. However this approach is limited by the stability criteria for explicit solutions of the diffusion equation: numerical instabilities would appear as the diffusion coefficient increased [9]. Alternatively, standard finite difference or finite element methods could be applied directly to (19); however these methods are limited by the well-known Peclet number restriction ($Pe = u\Delta x/D \leqslant 2$) [47] and perform poorly under advection dominated conditions (Fig. 1). Neither of these alternative options for solving the ADE permit the range of Peclet numbers

shown in Fig. 1 with a fixed discretisation. Therefore, incorporating the OS step into the KT algorithm enables an accurate and flexible methodology for solving combined advection–diffusion problems.

Historically, it has been common for numerical simulations of advection–diffusion type migration in mathematical biology to be conducted with standard Eulerian (finite difference or finite element) numerical algorithms. Therefore, these algorithms are subject to the Peclet number restrictions and associated errors shown in Fig. 1 for the important case of advection (chemotaxis/haptotaxis) dominant migration. These standard Eulerian approaches have been used for simulating migration on nongrowing domains [2,20,28] as well as migration on growing domains [6–8,21,36]. These limitations were recognized by Marchant et al. [24], who developed a Kurganov–Tadmor [19] central scheme for the solution of haptotaxis dominant migration on a nongrowing domain. This previous work was limited to nongrowing domains with small diffusivities [24]. These limitations are overcome in the present work by developing an algorithm applicable to either nongrowing, uniformly growing, or nonuniformly growing domains with migration being either purely diffusive, purely chemotactic (haptotactic) or any combination of chemotaxis (haptotaxis) and diffusion.

2.6. Migration on a uniformly growing domain: remarks on previous approaches

A uniformly growing domain is one where the local expansion rate does not depend on position in the domain. However, the local expansion rate can still be a function of time. For simplicity, in this case we write

$$\frac{\partial v}{\partial x} = \mu(t). \tag{22}$$

Substitution into Eq. (9) gives

$$\frac{\partial v}{\partial x} = \mu(t) = \frac{1}{L}\frac{\mathrm{d}L}{\mathrm{d}t}. \tag{23}$$

Eq. (23) can be interpreted in two ways. If the domain growth is known to be uniform and if the form of $\mu(t)$ can be estimated, then $L(t)$ can be determined from the differential equation (23). In reality, however, it is more likely that the domain growth is assumed to be uniform, L can be experimentally measured at different times, and then the exact nature of $\mu(t)$ can be deduced from (23).

Only for the special case $\mu(t) = \alpha$, a constant for all time, (so that $\partial v/\partial x$ is independent of both x and t), does Eq. (23) imply that $L(t)$ grows exponentially in time, as $L(t) = \mathrm{e}^{\alpha t}$. Alternative forms of $L(t)$, including linear and logistic functions [6,21] are possible under uniform growth conditions, provided that $\mu(t)$ varies in a specific way with time.

Without any loss of generality, we assume that the domain is elongating in the positive x direction, with the origin fixed so that $v(0, t) = 0$. By integrating (23), the velocity field associated with uniform growth is [6,7,21]:

$$v = \frac{x}{L}\frac{\mathrm{d}L}{\mathrm{d}t}. \tag{24}$$

Transforming this velocity field into the ξ coordinate and substituting into the conservation equations (10)–(11), yields the governing equations relevant for uniform growth on a transformed domain. For this

case, the hyperbolic terms associated with the transformation and domain growth cancel:

$$\frac{\partial n}{\partial t} = \frac{\partial}{\partial \xi}\left(\frac{D_n}{L^2}\frac{\partial n}{\partial \xi}\right) - \frac{\partial}{\partial \xi}\left(\frac{\chi}{L^2} n \frac{\partial g}{\partial \xi}\right) + n(1-n) - \frac{\dot{L}}{L} n, \tag{25}$$

$$\frac{\partial g}{\partial t} = \frac{\partial}{\partial \xi}\left(\frac{D_g}{L^2}\frac{\partial g}{\partial \xi}\right) + \beta(1-g) - \gamma n g - \frac{\dot{L}}{L} g. \tag{26}$$

The combination of uniform growth and the transformation gives a kinetic term that represents uniform dilution. The kinetic term can be easily incorporated into a numerical scheme without any severe limitation imposed by numerical accuracy considerations. We remark that the application of the KT-OS scheme to (25)–(26) is simpler than for the general system (10)–(11) as only three variables need to be conserved in the KT algorithm rather than six.

The simplifications associated with uniform growth mean that standard Eulerian numerical techniques are better suited under these conditions as there are less hyperbolic terms to be discretised. The presence of hyperbolic terms is of particular concern because of the Peclet number restrictions associated with traditional schemes. In the case of purely diffusive migration and uniform growth, (25) with $\chi = 0$, a standard numerical discretisation would be convenient as there are no hyperbolic terms and therefore no Peclet number restriction. For chemotactic migration on a uniformly growing domain, some diffusion must be included before standard numerical algorithms are applied [21]. This is a serious limitation of Eulerian algorithms, particularly for the important and relevant case where chemotaxis dominates diffusion. For migration of neural crest cells in the developing gut of vertebrate embryos, the growth is nonuniform [31] and the migration is predominantly chemotactic [46]; therefore, the applicability of traditional algorithms is severely limited. This observation has motivated the development of the KT-OS algorithm for such problems.

The numerical simplifications offered by invoking uniform domain growth (25)–(26) are obtained regardless of the form of $L(t)$. In order to proceed a choice of $L(t)$ must be made. As noted, linear, exponential and logistic models for $L(t)$ have been considered previously [6,21]. Laboratory observations indicate that gut growth in vertebrate embryos is approximately exponential [31]; therefore $L(t) = \mathrm{e}^{\alpha t}$ is used for presenting results in the next subsection.

2.7. Chemotactic and diffusive cell migration: inter-code comparison with a finite element algorithm

To demonstrate the accuracy of the full chemotactic and diffusive migration algorithm, a uniform growth and a nonuniform growth case are presented. Unfortunately, under these conditions there is no possibility of testing the numerical results against an analytical solution as carried out for the Gaussian hill problem. Therefore, an inter-code comparison is the best option for model testing in these cases [41].

For nonuniform growth an example is chosen to be numerically insightful. We focus on the case where the spatial dependence of $\partial v/\partial x$ is linear in x:

$$\frac{\partial v}{\partial x} = \kappa(t) x. \tag{27}$$

Substitution into Eq. (9) gives an expression for $\kappa(t)$ in terms of L and hence we obtain

$$\frac{\partial v}{\partial x} = \frac{2x}{L^2}\frac{\mathrm{d}L}{\mathrm{d}t}. \tag{28}$$

Integrating (28) with zero velocity at the origin gives a quadratic velocity field:

$$v = \left(\frac{x}{L}\right)^2 \frac{\mathrm{d}L}{\mathrm{d}t}. \tag{29}$$

Simulating growth with (29) does not permit cancellation of any terms in the transformed conservation equations (10)–(11). Therefore, this test case is suitable to detect the ability of a numerical algorithm to handle non-uniform growth conditions.

To complete the model description, the temporal growth $L(t)$ must be specified. We choose $L(t) = \mathrm{e}^{\alpha t}$. Consequently, we will compare two different velocity fields, one uniform (24), the other nonuniform (29), both having the same net exponential elongation. We next consider solving the full system (10)–(11) for these two cases.

To conduct the inter-code comparison, the Galerkin FE algorithm used to solve the full system (10)–(11) incorporates linear elements and mass lumping for the temporal and kinetic terms [22,37]. The FE algorithm was developed using standard techniques [37] and so the details are not presented. A backward Euler scheme is used for the temporal integration, and Picard iteration is used to solve the nonlinear equations. Picard iterations are conducted until $\max_i |c_i^{m+1} - c_i^m| < 1 \times 10^{-4}$, where c is the concentration of n or g, m is the iteration level and i is the nodal index. The key limitation of the FE algorithm is $Pe = \lambda \Delta\xi / D \leqslant 2$, where λ is the maximum propagation speed associated with the hyperbolic terms and $\Delta\xi$ is the grid spacing. The presence of nonlinear terms in the conservation system complicates the expression for the Peclet number. Therefore, we rely on the generation of grid-independent results to indicate that numerical error conditions are satisfied.

Initial conditions on $0 < x < 1$ are chosen to reflect an initial penetration of cells, at capacity density, into the growing end of the domain. The initial chemoattractant concentration represents uniformly saturated conditions, namely:

$$g(x, 0) = 1, \quad n(x, 0) = H(x - (1 - \varepsilon)), \tag{30}$$

where H is the Heaviside step-function and ε is the length of the domain initially colonised. The boundaries are closed to diffusive fluxes. The KT-OS and FE algorithms are used to generate the cell density and chemoattractant concentration profiles shown in Fig. 2.

The key result from the benchmarking exercise is that the profiles given by the FE and KT-OS algorithms are indistinguishable. The FE algorithm gave identical results with $\Delta\xi$ and Δt halved, indicating that the results are accurate and grid-independent. Now that the KT-OS algorithm is shown to properly account for chemotactic and diffusive migration on a non-uniformly growing domain, the algorithm can be used with confidence in other situations such as purely chemotactic migration with nonuniform growth.

Comparing profiles in Fig. 2a and 2b highlight some important differences between uniform and nonuniform growth. The most striking difference is that the advancing cell front in the quadratic growth case is more successful at colonising the domain. This is easily explained by considering the differences in the magnitude of the domain velocity for the two growth models. At any point in the domain, the domain velocity associated with the quadratic growth model is always a factor of x/L smaller than uniform growth so that net cell migration is more effective on the quadratically growing domain. The dilution associated with the domain growth, given by the terms $\frac{1}{L}\frac{\partial v}{\partial \xi} n$ and $\frac{1}{L}\frac{\partial v}{\partial \xi} g$ in (10)–(11), is also quite different. The difference in dilution is most clearly demonstrated in the chemoattractant profiles in Fig. 2. In the region to the left of the advancing cell profile the dilution is spatially uniform for uniform growth (Fig. 2a), while the profiles for nonuniform growth reveal a spatially variable dilution effect (Fig. 2b).

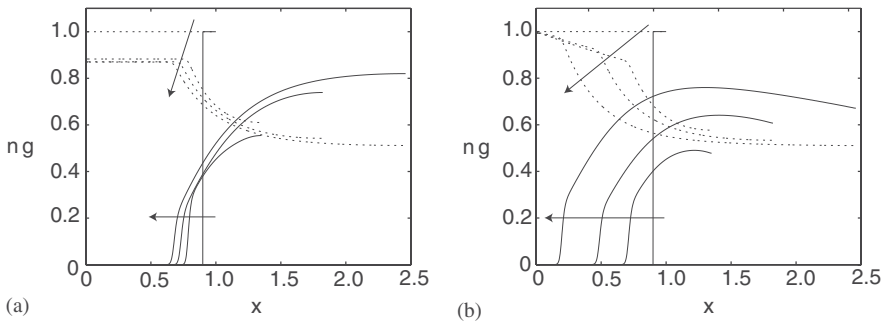

Fig. 2. Inter-code comparison for chemotactic and diffusive migration with $L(t) = e^{\alpha t}$ under (a) uniform growth conditions and, (b) quadratic growth conditions. Results are shown for n (solid line) and g (dotted line) at $t = 0, 2, 4, 6$ with the arrows showing the direction of increasing time. Parameter values are $\beta = \gamma = 1$, $D_n = D_g = 1 \times 10^{-3}$, $\chi = 1 \times 10^{-1}$, $\alpha = 0.15$, $\varepsilon = 0.1$. Numerical solutions are computed using $\Delta\xi = \Delta t = 1 \times 10^{-3}$. Profiles are plotted in the x coordinate to emphasise the domain growth.

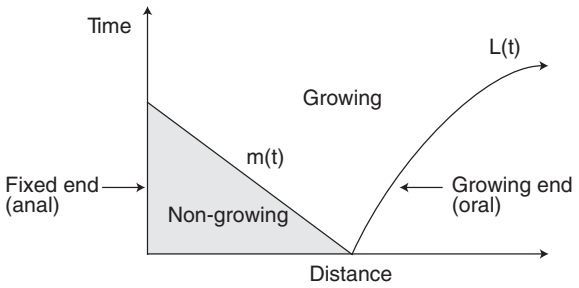

Fig. 3. Schematic of the nonuniform travelling wave-of-growth. The domain elongates according to $L(t)$ while the travelling wave $m(t)$ traverses from the growing end across the domain to the fixed end delineating the nongrowing region (shaded) from the growing region (unshaded). The case where $m(0) = L(0) = 1$ is shown here.

3. Applying the KT-OS algorithm to the development of the enteric nervous system

During embryogenesis, the entire tissue substrate may not always commence growing at the same time. This kind of growth is relevant to the migration of neural crest cells along the gut in the development of the enteric nervous system. Neural crest cells enter the oral end of the gut and migrate towards the anal end simultaneously as the gut grows. The oral end of the gut grows, primarily by elongation, before the anal end, thereby giving rise to nonuniform domain growth [21,31]. Here we propose a mathematical model of nonuniform growth relevant to the developing gut.

Fig. 3 is a conceptual model for embryonic gut growth motivated by the measurements in [31]. At any time, the domain can be divided into two sections: (1) the growing (oral) end which is elongating, and (2) the fixed (anal) end which is not growing [31]. It is assumed that a wave-of-growth, delineating growing and nongrowing sections of tissue, travels with some velocity across the domain. The front of the wave-of-growth is at $x = m(t)$ and moves in the negative direction until it reaches the origin, after which time the whole domain is growing. We assume that the growing part $m(t) < x < L(t)$ elongates with $\partial v/\partial x = \alpha$, a constant independent of both position and time. This means that the domain growth in

this growing region is the simplest type of uniform growth. The constant α is the rate of expansion of the underlying tissues through proliferation.

This type of nonuniform growth can be mathematically described by

$$\frac{\partial v}{\partial x} = \alpha H(x - m(t)) \quad \text{for } 0 < x < L(t), \tag{31}$$

where $m(t)$ is a decreasing function. Hence $H(x - m(t))$ represents a step-function travelling wave moving to the left. The rate of elongation of the domain is

$$\frac{\mathrm{d}L}{\mathrm{d}t} = \int_0^{L(t)} \frac{\partial v}{\partial x}\,\mathrm{d}x = \begin{cases} 0 & \text{when } m(t) > 0 \text{ and } 0 < x < m(t), \\ \alpha(L(t) - m(t)) & \text{when } m(t) > 0 \text{ and } m(t) < x < L(t), \\ \alpha L(t) & \text{when } m(t) = 0. \end{cases} \tag{32}$$

To interpret (32) we assume that $m(t)$ and α are measurable. Therefore, the domain elongation $L(t)$ is uniquely determined by (32). The frame of reference for the problem is prescribed so that $x = 0$ remains fixed. For these conditions the velocity field is

$$v(x,t) = \begin{cases} 0 & \text{when } m(t) > 0 \text{ and } 0 < x < m(t), \\ \alpha(x - m) & \text{when } m(t) > 0 \text{ and } m(t) < x < L(t), \\ \alpha x & \text{when } m(t) = 0. \end{cases} \tag{33}$$

This nonuniform growth model is applicable for $0 \leqslant m(0) \leqslant 1$; in this work the particular case $m(0) = 1$ is examined. For simplicity, we assume the velocity of the wave-of-growth to be linear:

$$m(t) = (1 - bt)H(1 - bt). \tag{34}$$

Eqs. (33) and (34) specify the domain growth as a function of the speed of the travelling wave b and the growth rate α. The domain length is

$$L(t) = \begin{cases} \dfrac{b}{\alpha}\mathrm{e}^{\alpha t} + \left(1 - \frac{b}{\alpha}\right) - bt, & 0 < t < \dfrac{1}{b}, \\ \left[\dfrac{b}{\alpha}\mathrm{e}^{\frac{\alpha}{b}} - \dfrac{b}{\alpha}\right]\mathrm{e}^{\alpha(t - \frac{1}{b})}, & t > \dfrac{1}{b}. \end{cases} \tag{35}$$

Thus L behaves exponentially for later times, consistent with experimental measurements [31].

The nonuniform growth model (31)–(35) shall now be incorporated into the KT-OS algorithm to investigate migration in conjunction with the nonuniform domain growth.

3.1. Effect of nonuniform travelling wave-of-growth on the chemoattractant distribution

To examine the influence of nonuniform growth on the dynamics of n and g, it is insightful to first simulate an uncoupled problem where the dynamics of g are independent of n. The uncoupling is achieved by setting $\gamma = 0$ and we further simplify the system by assuming diffusive migration is negligible, $D_g = 0$. Under these conditions the conservation equation for g is:

$$\frac{\partial g}{\partial t} = -\frac{\partial}{\partial x}(vg) + \beta(1 - g), \tag{36}$$

on the domain $0 < x < L(t)$. Here, the domain velocity v is nonuniform and given by (33)–(34).

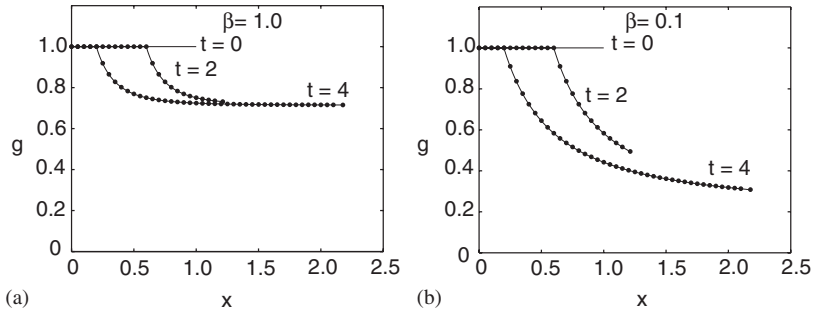

Fig. 4. Comparison of numerical (solid line) and the MOC analytical (•) solutions showing the dilution effects of nonuniform growth upon g. Results are presented for (a) high production conditions $\beta = 1.0$, and (b) low production conditions $\beta = 0.1$. The nonuniform growth parameters are $\alpha = 0.4$ and $b = 0.2$; numerical solutions are for $\Delta\xi = 1 \times 10^{-3}$ and $\Delta t = 5 \times 10^{-3}$. Profiles are reported in the x coordinate to emphasise the domain growth.

The method of characteristics (MOC) is used to solve (36) and demonstrate the interactions between nonuniform dilution and chemoattractant production. This exercise provides a final test for the KT-OS algorithm. A characteristic is a curve that satisfies $\mathrm{d}x/\mathrm{d}t = v(x,t)$. Along a characteristic g is governed by

$$\frac{\mathrm{d}g}{\mathrm{d}t} = \beta(1-g) - g\,\frac{\partial v}{\partial x}. \tag{37}$$

As the growth is nonuniform the dilution term $g\partial v/\partial x$ depends on position. To solve (37), we consider a characteristic starting at $x(0) = x_0$ on $0 < x_0 < 1$, with $g(x_0, 0) = G_0$. Along a characteristic the concentration of g is

$$g(t) = \begin{cases} (G_0 - 1)\mathrm{e}^{-\beta t} + 1, & 0 < t < t_0 = \dfrac{1-x_0}{b}, \\ \left[(G_0 - 1)\mathrm{e}^{-\beta t_0} + \dfrac{\alpha}{\beta+\alpha}\right]\mathrm{e}^{(\beta+\alpha)(t_0-t)} + \dfrac{\beta}{\beta+\alpha}, & t > t_0. \end{cases} \tag{38}$$

Numerical and analytical results with $G_0 = 1$ are computed for high and low production rates to demonstrate the interplay between the production kinetics and dilution. Fig. 4 illustrates that the numerical and analytical profiles of g are identical. The initially saturated part of the domain retreats as the wave-of-growth sweeps across the domain. The steady value of g is $\beta/(\beta+\alpha)$. For high production, this equilibrium value is attained rapidly after the wave-of-growth passes. Alternatively, for low production the equilibrium concentration is much smaller and the profiles do not reach a steady state for the times considered. This uncoupled analysis gives some insight into the interactions between the domain growth dynamics and the chemoattractant production rate for a coupled migration problem ($\gamma > 0$).

3.2. Chemotactic migration upon a nonuniformly growing domain with a wave-of-growth

To investigate the influence of the travelling wave-of-growth on the migration characteristics of a cell population, it is necessary to solve (10)–(11) in conjunction with the nonuniform growth condition (33)–(34). This kind of problem is easily handled by the KT-OS scheme for any combination of diffusion or chemotactic migration.

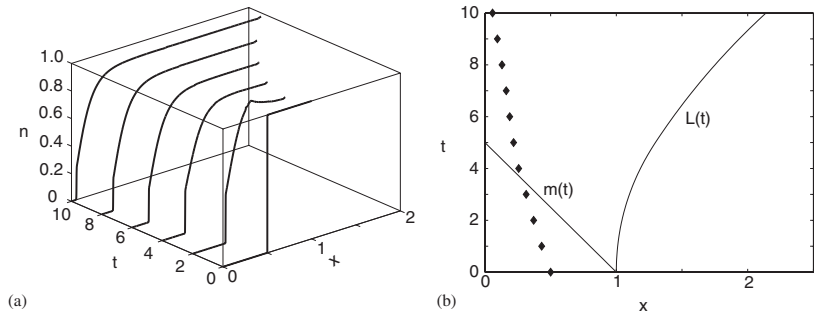

Fig. 5. Numerical results showing (a) the profile of n and (b) the progression of the $n = 0.1$ contour (♦) with the length of the domain $L(t)$ and the position of the transition to growth $m(t)$. Nonuniform growth parameters are $b = 0.2$, $\alpha = 0.1$. Migration parameters are $\chi = 1 \times 10^{-2}$, $D_n = D_g = 0$ and $\beta = \gamma = 1$. Initial penetration of cells is $\varepsilon = 0.5$. Numerical computations are performed with $\Delta\xi = 1 \times 10^{-3}$ and $\Delta t = 5 \times 10^{-3}$.

To demonstrate a range of behaviours, results from three simulations are presented. All simulations are performed with $\chi = 1 \times 10^{-2}$ and $D_n = D_g = 0$ as we are primarily interested in the case where chemotaxis is the dominant migration mechanism [46]. The initial conditions are a uniformly saturated chemoattractant concentration and a localised cell concentration, namely Eq. (30). Zero flux boundary conditions are prescribed. Results are computed until $t = 10$ and the n profiles are shown in Fig. 5.

Fig. 5a shows the progression of the migratory population of cells. The elongation of the domain and associated dilution of the cell concentration in the growing region are clear. At early times the advancing front develops a discontinuity. This is expected as discontinuous solutions for chemotactic migration are known to occur when the initial distribution of cells has compact support on a nongrowing domain [20,22,25]. The migration continues towards the origin until $t = 10$ when the domain is practically colonised. The interaction of the nonuniform growth, the elongation of the domain, and the advancement of the cell front are summarised in Fig. 5b. For early times, the $n = 0.1$ contour advances rapidly towards the origin. At later times, once the wave-of-growth passes the cell front, the advancement is slowed. The slowed front continues to migrate towards the origin and the entire domain becomes populated just after $t = 11$. We also remark that the n profile shows a local maximum when $t = 2$; this observation will be explained after the next example.

A second example is shown in Fig. 6 where the same problem is solved but for a much stronger growth rate, $\alpha = 0.3$. Fig. 6a shows the progression of the cell population. During the time interval $0 < t < 10$ the domain elongates to over ten times the original length; to maintain clarity, the profiles are truncated to show only $0 < x < 5$. For early times the cells migrate toward the origin until the wave-of-growth overtakes the advancing cells. Once this occurs the migration slows, halts, and is then swept in the opposite direction due to the magnitude of the domain growth. After the front moves in the positive x direction the domain will never be colonised. This interplay between the advancing cell front, the travelling wave-of-growth and the domain elongation is summarised in Fig. 6b.

For both cases presented so far, there is a spatially localised maximum in the n profile at $t = 2$. This phenomena is caused by the combination of chemotactic migration and the nonuniform dilution of g. As the wave-of-growth travels across the domain, the chemoattractant profile dilutes in a non-uniform manner (Fig. 4). Ahead of the wave there is no chemotactic flux. Conversely, just behind the wave, a growth-induced chemotactic gradient exists due to dilution. Therefore, in this region, there is a local

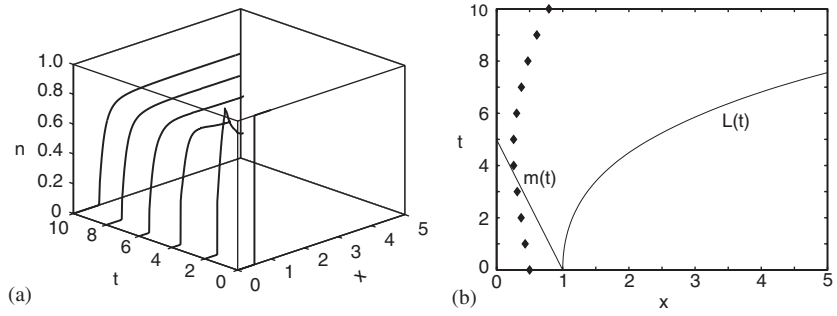

Fig. 6. Numerical results showing (a) the profile of n and (b) the progression of the $n = 0.1$ contour (♦) with the length of the domain $L(t)$ and the position of the transition to growth $m(t)$. Nonuniform growth parameters are $b = 0.2$, $\alpha = 0.3$. Migration parameters are $\chi = 1 \times 10^{-2}$, $D_n = D_g = 0$ and $\beta = \gamma = 1$. Initial penetration of cells is $\varepsilon = 0.5$. Numerical computations are performed with $\Delta\xi = 1 \times 10^{-3}$ and $\Delta t = 5 \times 10^{-3}$.

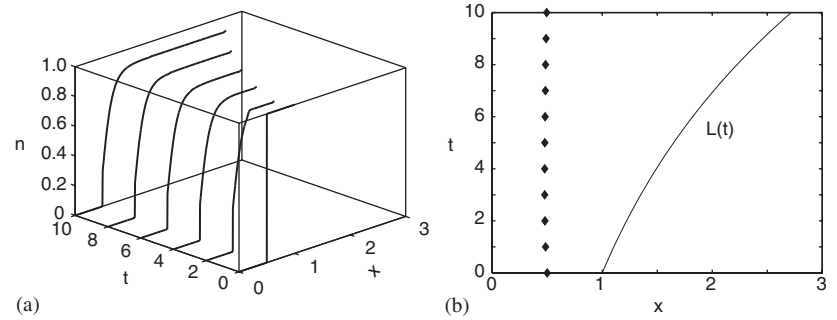

Fig. 7. Numerical results showing (a) the profile of n and (b) the progression of the $n = 0.1$ contour (♦) with the length of the domain $L(t)$. Nonuniform growth parameters are $b = 1000$, $\alpha = 0.1$. Migration parameters are $\chi = 1 \times 10^{-2}$, $D_n = D_g = 0$ and $\beta = \gamma = 1$. Initial penetration of cells is $\varepsilon = 0.5$. Numerical computations are performed with $\Delta\xi = 1 \times 10^{-3}$ and $\Delta t = 5 \times 10^{-3}$.

chemotactic flux of n into the negative x direction. This combination of a growth-induced dilution of g and chemotactic migration of n gives rise to a localised region where there is a net chemotactic flux of n into that region. According to mass-conservation principles, n must increase in this region. The formation of the local maximum dissipates in time as the travelling wave-of-growth is continuously moving toward the origin.

A final example is shown in Fig. 7. where essentially the same problem as in Fig. 5 is solved. The key difference is that the speed of the travelling wave-of-growth is sufficiently exaggerated that the nonuniform growth converts almost instantaneously into uniform growth. Although the shape of the cell profile behind the front changes appreciably, the cell front is practically unable to move against the domain growth. This is because the wave-of-growth almost instantaneously traverses the domain thereby making progress of the migration very difficult. At early times the position of the $n = 0.1$ contour makes a small advancement towards the origin. At later times the contour is slowly swept in the positive x direction precluding colonisation.

These three simulations show that in order to realistically model cell migration on a nonuniformly growing domain, the spatial and temporal nature of the non-uniform growth must be accurately identified as the form of the growth can dictate colonisation success or failure. This observation further generalises the analysis of [21]. This previous work observed that the colonisation of a uniformly growing domain, where migration is primarily chemotactic, is controlled by χ/α and ε. These parameters, together with those governing the nonuniform growth, will also be relevant to colonisation problems on nonuniformly growing domains.

In general, the nonuniform travelling wave-of-growth model is applicable for all situations where $0 < m(0) < 1$ and $b > 0$. Care should be exercised in the special case where $b = 0$ and $\chi > 0$. In this case, the domain is divided into a growing and nongrowing region, and $m(0)$ remains fixed. The dilution due to domain growth will be discontinuous causing the distribution of chemoattractant to contain a discontinuity. Therefore, the chemotactic gradient and flux become infinite at $m(0)$. This can be remedied by ensuring that $\partial v/\partial x$ is continuous. A simple way of doing this is to introduce a narrow region where $\partial v/\partial x$ is a linear ramp across $m(0)$.

4. Discussion and conclusions

The numerical algorithm developed here provides a significant advance upon previous attempts to simulate migration on growing domains. Prior studies have been largely restricted to uniform growth [6,8,21,36]. Simulating uniform growth on a transformed domain yields an important numerical simplification. For uniform growth the hyperbolic terms associated with domain growth and the transformation cancel; thereby leaving growth represented as a straightforward kinetic term [21]. Therefore, in the case of diffusive migration on a uniformly growing domain the conservation equation is purely diffusive in the transformed coordinate and easily solved using standard numerical techniques.

The inclusion of chemotaxis is important for two reasons. Firstly, for some cell migration problems, chemotaxis is the dominant migration mechanism [21,46]. Secondly, the inclusion of chemotaxis means that the numerical algorithm must be capable of resolving the nonlinear hyperbolic term associated with chemotactic migration. Conducting numerical simulations of chemotactic migration on a nonuniformly growing domain is challenging because of the predominance of hyperbolic terms in the conservation equations.

Previous attempts at solving chemotaxis (haptotaxis) dominated problems, either on a growing or a nongrowing domain, have generally involved the use of standard Eulerian numerical algorithms where linear diffusion is included, in part, to preclude numerical errors [2,20,21,28,36]. Diffusion is typically included by using a centered difference for the advection term and explicitly adding a linear diffusion term [20,21], or alternatively diffusion is introduced numerically by using an upstream difference for the advection term [47]. Adding linear diffusion to a standard numerical algorithm to overcome numerical errors is problematic for two reasons. Firstly, recent numerical work investigating the interaction between diffusive and chemotactic migration on a nongrowing domain showed that a very small amount of diffusion can completely mask the presence of chemotaxis [22]. Therefore by adding diffusion to a chemotaxis simulation in order to overcome numerical errors, it is likely that the chemotactic characteristics of the system are completely, albeit inadvertently, concealed. Secondly, adding diffusion in an ad hoc manner is imprudent because cell diffusivities are infrequently known or measured a priori. For example, several diffusive migration models including pattern formation [17] and cell invasion [23] have been related to realistic biological observations without any specific knowledge of the diffusivity.

Using a central scheme to solve a chemotaxis problem on a nonuniformly growing domain is a useful approach for overcoming the standard problems associated with the numerical solution of hyperbolic conservation systems. In particular, the KT central scheme is known to perform well for nonlinear hyperbolic problems [19,22]. Previous attempts at using the KT algorithm for problems including diffusion suggested that the diffusion term be discretised explicitly [19,24]. This approach is only applicable when the diffusion coefficient is small. The objective of the present work was to develop an algorithm for simulating cell migration for any combination of diffusion and chemotaxis. This flexibility is achieved with an OS step. This approach is ideal for interpreting laboratory observations of migration where the relative contributions of diffusion and chemotaxis are initially unknown.

Acknowledgements

The authors gratefully acknowledge the support of a National Health and Medical Research Council project grant ID237144. Kerry Landman also thanks the Particulate Fluids Processing Center, an Australian Research Council ARC Special Research Center, for support.

References

[1] J. Adler, Chemotaxis in bacteria, Science 153 (1966) 708–716.
[2] A.R.A. Anderson, M.A.J. Chaplain, Continuous and discrete mathematical models of tumor-induced angiogenisis, B Math. Biol. 60 (1998) 857–900.
[3] S. Aznavoorian, M.L. Stracke, H. Krutzsch, E. Schiffmann, L.A. Liotta, Signal transduction for chemotaxis and haptotaxis by matrix molecules in tumor-cells, J. Cell. Biol. 110 (1990) 1427–1438.
[4] S. Berres, R. Bürger, K.H. Karlsen, Central schemes and systems of conservation laws with discontinuous coefficients modeling gravity separation of polydisperse suspensions, J. Comput. Appl. Math. 164 (65) (2004) 53–80.
[5] R. Blakemore, Magnetotactic bacteria, Science 190 (1975) 377–379.
[6] E.J. Crampin, E.A. Gaffney, P.K. Maini, Reaction and diffusion on growing domains: scenarios for robust pattern formation, B Math. Biol. 61 (1999) 1093–1120.
[7] E.J. Crampin, W.W. Hackborn, P.K. Maini, Pattern formation in reaction-diffusion models with nonuniform domain growth, B Math. Biol. 64 (2002) 747–769.
[8] E.J. Crampin, P.K. Maini, Modelling biological pattern formation: the role of domain growth, Comments on Theoret. Biol. 6 (2001) 229–249.
[9] J. Crank, The Mathematics of Diffusion, second ed., Oxford University Press, Oxford, England, 1975.
[10] R. Dillon, H.G. Othmer, A mathematical model for outgrowth and spatial patterning of the vertebrate limb bud, J. Theoret. Biol. 197 (1999) 295–330.
[11] J. Donea, A. Huerta, Finite Element Methods for Flow Problems, Wiley, West Sussex, England, 2003.
[12] R.A. Fisher, The wave of advance of advantageous genes, Annu. Eugenic. 7 (1937) 355–369.
[13] U. Goerke, A.H.L. Chamberlain, E.A. Crilly, P.J. McDonald, Model for water transport into powdered xanthan combining gel swelling and vapour diffusion, Phys. Rev. E 62 (2000) 5353–5359.
[14] G. Gottardi, M. Venutelli, Central schemes for open channel flow, Int. J. Numer. Meth. Fl. 41 (2003) 841–861.
[15] C.J. Hearn, M. Murphy, D.F. Newgreen, GDNF and ET-3 differentially modulate the numbers of avian enteric neural crest cells and enteric neurons in vitro, Dev. Biol. 197 (1998) 93–105.
[16] E.F. Keller, L.A. Segel, Model for chemotaxis, J. Theoret. Biol. 30 (1971) 225–234.
[17] S. Kondo, R. Asai, A reaction-diffusion wave on the skin of the marine angelfish *Pomacanthus*, Nature 376 (1995) 765–768.
[18] P.M. Kulesa, G.C. Cruywagen, S.R. Lubkin, P.K. Maini, J. Sneyd, M.W.J. Ferguson, J.D. Murray, On a model mechanism for the spatial patterning of teeth primordia in the alligator, J. Theoret. Biol. 180 (1996) 287–296.

[19] A. Kurganov, E. Tadmor, New high-resolution central schemes for nonlinear conservation laws and convection–diffusion equations, J. Comput. Phys. 160 (2000) 241–282.
[20] K.A. Landman, G.J. Pettet, D.F. Newgreen, Chemotactic cellular migration: smooth and discontinuous travelling wave solutions, SIAM J. Appl. Math. 63 (2003) 1666–1681.
[21] K.A. Landman, G.J. Pettet, D.F. Newgreen, Mathematical models of cell colonization of uniformly growing domains, B. Math. Biol. 65 (2003) 235–262.
[22] K.A. Landman, M.J. Simpson, J.L. Slater, D.F. Newgreen, Diffusive and chemotactic cellular migration: smooth and discontinuous travelling wave solutions, SIAM J. Appl. Math. 65 (2005) 1420–1442.
[23] P.K. Maini, D.L.S. McElwain, D. Leavesley, Travelling waves in a wound healing assay, Appl. Math. Lett. 17 (2004) 575–580.
[24] B.P. Marchant, J. Norbury, J.A. Sherratt, Travelling wave solutions to a haptotaxis-dominated model of malignant invasion, Nonlinearity 14 (2001) 1653–1671.
[25] B.P. Marchant, J. Norbury, Discontinuous travelling wave solutions for certain hyperbolic problems, IMA J. Appl. Math. 67 (2002) 201–224.
[26] H. Meinhardt, Models of Biological Pattern Formation, Academic Press, London, 1982.
[27] J.D. Murray, Mathematical Biology, second ed., Springer, New York, 2003.
[28] M.R. Myerscough, P.K. Maini, K.J. Painter, Pattern formation in a generalized chemotactic model, B Math. Biol. 60 (1998) 1–26.
[29] D. Natarajan, C. Marcos-Gutierrez, V. Pachnis, E. de Graaff, Requirement of signalling by receptor tyrosine kinase RET for the directed migration of enteric nervous system progenitor cells during mammalian embryogenesis, Development 129 (2002) 5151–5160.
[30] D.F. Newgreen, C.A. Erikson, The migration of neural crest cells, Int. Rev. Cytol. 103 (1986) 89–145.
[31] D.F. Newgreen, B. Southwell, L. Hartley, I.J. Allan, Migration of enteric neural crest cells in relation to growth of the gut in avian embryos, Acta. Anat. 157 (1996) 105–115.
[32] S.A. Newman, H.L. Frisch, Dynamics of skeletal pattern formation in developing chick limb, Science 205 (1979) 662–668.
[33] W. Orr, J. Varani, M.D. Gondek, P.A. Ward, G.R. Mundy, Chemotactic responses of tumor cells to products of resorbing bone, Science 203 (1979) 176–179.
[34] H.G. Othmer, A. Stevens, Aggregation, blowup, and collapse: the ABC's of taxis in reinforced random walks, SIAM J. Appl. Math. 57 (1997) 1044–1081.
[35] K.J. Painter, Chemotaxis as a mechanism for morphogenisis, Ph.D. Thesis, University of Oxford, Oxford, UK, 1997.
[36] K.J. Painter, P.K. Maini, H.G. Othmer, Stripe formation in juvenile *Pomacanthus* explained with a general Turing mechanism with chemotaxis, P. Natl. Acad. Sci. USA 96 (1999) 5549–5554.
[37] L.J. Segerlind, Applied Finite Element Analysis, second ed., Wiley, Singapore, 1984.
[38] T. Sekimura, A. Madzvamuse, A.J. Wathen, P.K. Maini, A model for colour pattern formation in the butterfly wing of *Papilio dardanus*, P. Roy. Soc. Lond. B Bio. 267 (2000) 851–859.
[39] C.-W. Shu, S. Osher, Efficient implementation of essentially non-oscillatory shock-capturing schemes, J. Comput. Phys. 77 (1998) 439–471.
[40] B.R. Simon, J.P. Liable, D. Pflaster, Y. Yuan, M.H. Krag, A poroelastic finite element formulation including transport and swelling in soft tissue structures, J. Biomech. Eng.-T ASME 118 (1996) 1–9.
[41] M.J. Simpson, T.P. Clement, Theoretical analysis of the worthiness of the Henry and Elder problems as benchmarks of density-dependent groundwater flow models, Adv. Water Resour. 26 (2003) 17–31.
[42] M.J. Simpson, K.A. Landman, T.P. Clement, Assessment of a non-traditional operator split algorithm for simulation of reactive transport Math Comput Simulat, 2005, in press.
[43] G. Strang, On the construction and comparison of difference schemes, SIAM J. Numer. Anal. 5 (1968) 506–517.
[44] G. Taraboletti, D.D. Roberts, L.A. Liotta, Thrombospondin-induced tumor-cell migration-haptotaxis and chemotaxis are mediated by different molecular domains, J. Cell. Biol. 105 (1987) 2409–2415.
[45] R.T. Tranquillo, Theories and models of gradient perception, in: J.P. Armitage, J.M. Lackie (Eds.), Biology of the Chemotactic Response, Cambridge University Press, Cambridge UK, 1990.
[46] H.M. Young, C.J. Hearn, P.G. Farlie, A.J. Canty, P.Q. Thomas, D.F. Newgreen, GDNF is a chemoattractant for enteric neural cells, Dev. Biol. 229 (2001) 503–516.
[47] C. Zheng, G.D. Bennett, Applied Contaminant Transport Modelling, second ed., Wiley, New York, USA, 2002.